Theor Chem Acc (2007) 117:827–845
DOI 10.1007/s00214-006-0204-3

REGULAR ARTICLE

Theory of oxides surfaces, interfaces and supported nano-clusters

Fabrizio Cinquini · Cristiana Di Valentin · Emanuele Finazzi · Livia Giordano · Gianfranco Pacchioni

Received: 14 June 2006 / Accepted: 13 October 2006 / Published online: 13 December 2006

Abstract Oxides surfaces and thin films are finding continuous new technological applications and represent an important class of systems in materials science. Today we assist to a considerable effort to characterize the surfaces and the interfaces of oxide materials at an atomistic level. The intense experimental activity in this field has stimulated a parallel computational activity based on high-quality first principle calculations. In this review we focus our attention on the properties of oxide surfaces, and we describe the main factors that contribute to determine their behaviour: (1) nature of the bonding and electronic structure of the oxide; (2) surface morphology and defectivity; (3) doping and functionalization; (4) redox properties; (5) nano-dimensionality (e.g. in ultra-thin films). We also show how each of these parameters can affect the properties of supported metal atoms and nano-particles.

Keywords Oxide surfaces · Metal–oxide interfaces · Metal clusters · Surface chemistry · Defects · Thin films

1 Introduction

Oxides surfaces and thin films are finding continuous new applications in advanced technologies like corrosion protection, thermal coating, in microelectronics for their dielectric properties; films of magnetic oxides are integral components in magnetic recording devices and many microporous materials are based on oxides. Today there is a considerable effort to characterize the surfaces and the interfaces of oxide materials at an atomistic level. New experimental methods allow to growth oxide films of various thickness on metal supports and to study their analogies and differences with crystalline and amorphous oxides [1–5]. This has opened the route towards a new class of materials with unprecedented properties often connected to the reduced dimensionality of the films. Furthermore, supported oxide thin films allows one to overcome the difficulties connected to the use of electron spectroscopies to study insulating oxides and also allows the detailed mapping of the surface via scanning tunneling microscopy (STM) images.

Well-characterized oxide supports can serve as model systems of supported metal catalysts [6,7]. To this end, new preparation techniques have been developed to deposit well defined and mono-dispersed metal clusters and to study their reactivity as a function of support, metal, cluster size, etc. [7]. In this way, complex catalytic processes can be divided into a series of elementary steps thus allowing a more detailed microscopic characterization. The increasing experimental activity has stimulated a parallel computational activity based on first principle calculations. Often it is only from a combined use of theory and experiment that the exact surface structure and the behavior of supported metal clusters have been identified.

Nowadays, first principle band structure calculations based on large supercells are routinely done and provide an essential complement to experiment to identify surface properties. Band structure calculations, usually based on plane waves basis sets and on the density functional theory (DFT) approach, represent the most appropriate computational method to study extended

F. Cinquini · C. Di Valentin · E. Finazzi · L. Giordano · G. Pacchioni (✉)
Dipartimento di Scienza dei Materiali,
Università di Milano-Bicocca,
Via R. Cozzi, 53, 20125 Milano, Italy
e-mail: gianfranco.pacchioni@unimib.it

solids. However, an alternative approach, the cluster approach, has been developed with the aim of describing in chemical terms interactions occurring at surfaces and other localized phenomena [8]. The design of appropriate cluster models to represent bulk solids or surfaces has been a central activity of our group in the past and has lead to several important results.

In this review we summarize through selected examples some general concepts on oxide surfaces, interfaces, and supported clusters. We provide a brief overview of a field of nanoscience that has the potential to produce spectacular results in the near future. We do not restrict the analysis to computational results, but we also illustrate important experimental aspects and discuss illustrative cases where the joint use of theory and experiment has permitted substantial advances in the field.

2 Computational models of surfaces

2.1 Periodic models

The electronic structure of solids is usually described in terms of band structure. A unit cell containing a given number of atoms is repeated periodically in three dimensions to account for the "infinite" nature of the crystalline solid and the Schrödinger equation is solved for the atoms in the unit cell subject to periodic boundary conditions. This approach can also be extended to adsorbates on surfaces by means of the supercell method in which an artificial periodic structure is created where the adsorbate is translationally reproduced in two directions of space, Fig 1a. This procedure allows the use of efficient computer programs either based on DFT and plane waves approaches [9] or on Hartree–Fock (HF) and post-HF based methods with localized atomic orbitals [10,11]. With the usual dimensions of the supercells, one models relatively high adsorbate coverage, from full monolayer, $\theta = 1$, to 1/8 of monolayer, $\theta = 0.125$, rarely below. The problem of the interaction between the adsorbates is usually negligible, except when the adsorbate is charged or induces a large surface dipole. The treatment of charged adsorbates with the supercell approach is feasible but requires to include dipole corrections to remove the long range Coulomb interaction between the charges [12], a procedure which is not always straightforward. Furthermore, the supercell approach is not suited to simulate highly disordered situations or sites characterized by low-symmetry such as defects or morphological irregularities.

2.2 Local cluster models

The alternative to the periodic band structure methods is the cluster model approach [8,13,14]. A finite number of atoms is used to describe a part of the surface, and the rest is treated in a simplified way (embedding), Fig. 1b. The main conceptual difference is that in the cluster approach one uses molecular orbitals, MO, instead of plane waves. The description of the electronic properties is thus done in terms of orbitals, allowing one to treat problems in solids with the typical language of chemistry, the language of orbitals. This is particularly useful when dealing with surface problems and with the reactivity of a solid surface. Of course, cluster models are not free from limitations and their use requires more experience than that of periodic approaches. The most serious drawback is that the effect of the surrounding is taken into account in an approximate way ("embedding"). The advantages are (1) the description of a very low coverage of adsorbates or concentration of defects; (2) the possibility to use accurate theoretical methods derived from quantum chemistry (explicitly correlated wave function based methods, like CI,

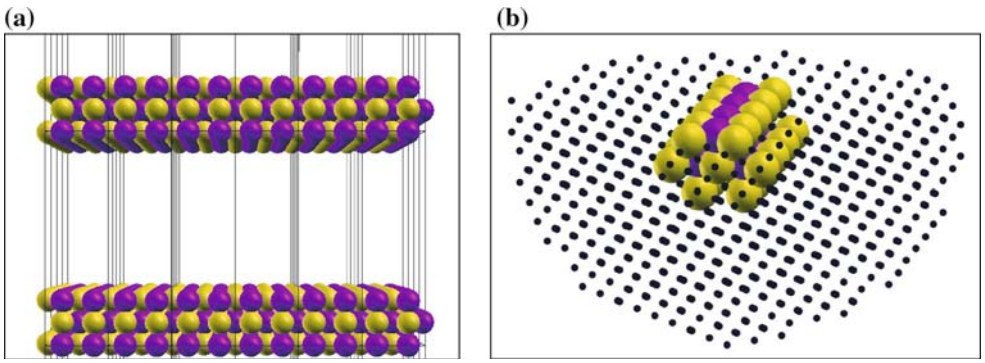

Fig. 1 Schematic representation of **a** a slab model and **b** an embedded cluster to represent an oxide surface. The spheres of different color represent cations and anions of the system; in the cluster model the quantum mechanical part is surrounded by a large array of classical ions (polarizabile ions, point charges, etc.)

MCSCF, CCSD(T), etc.); (3) the possibility to use hybrid DFT functionals (e.g. the popular B3LYP exchange-correlation functional, see Sect. 3.2) thus removing uncertainties connected to pure DFT functionals (see Sect. 3.3); (4) the possibility to compute optical spectra and excited states properties or (5) to treat properly spin states, EPR spectra and magnetic coupling interactions (particularly important for radical species, or defects with localized holes or electrons [15]). Some of these problems can be removed also by using periodic codes based on localized atomic orbital basis sets, like the CRYSTAL code developed over the past 20 years at the University of Torino [16].

2.3 Embedding schemes

Approximate embedding schemes have been proposed for oxide or inorganic materials. There are two limiting situations where embedding works satisfactorily, i.e. when the solid has a distinct ionic or covalent character. In the first case one has to include the Madelung potential of the extended crystal, in the second case to saturate the dangling bonds at the periphery of the quantum cluster. For example, in SiO_2, a covalent polar oxide, the cluster dangling bonds are often saturated by H atoms with satisfactory results [13] (but more elaborate embeddings have been developed, see below). Things become much more complex when one deals with semi-covalent oxides or with transition metal (TM) compounds where the oxidation state of the TM ion can change. In these cases the design of properly embedded clusters is problematic. In fact, few examples of this approach exist for the treatment of TM oxides. The model works provided that no charge transfer occurs between the adsorbed species and the surface; when this occurs charge may accumulate at the low-coordinated TM ions at the cluster border.

The embedding of ionic solids provides results fully comparable with those obtained from periodic models (see e.g. Sect. 6.2). A simple approach is to surround the quantum cluster by a large array of point charges (PC) to reproduce the Madelung field of the host [17]. Since positive PC's polarize the oxide anions at the cluster border and cause an incorrect behavior of the electrostatic potential [18], they are usually replaced by an effective core potential, ECP, with no basis functions representing the finite size of the cation core [19]. What is still missing is the polarization of the host crystal induced by an adsorbed species or by the presence of a defect. This effect can be particularly important for charged species. The polarization energy, E_{pol}, induced by a charge on the surrounding lattice of an insulator can be estimated by means of the classical Born formula [20]:

$$E_{pol} = -(1 - 1/\varepsilon)q^2/2R \quad (1)$$

where ε is the dielectric constant of the material, q is the absolute value of the charge and R is the radius of the spherical cavity where the charge is distributed. Since a certain degree of ambiguity remains in the definition of R, this correction is only qualitative [21]. In a more refined approach instead of PC's the cluster is surrounded by polarizable ions described according to the shell model approach [22,23] (here an ion is represented by a point core and a shell connected by a spring to simulate its dipole polarizability); in this way the polarization response of the host is taken into account self-consistently. In a recent extension [24,25] all quantum-mechanical, interface and classical ions (both cores and shells) are allowed to relax simultaneously in the course of geometry optimization, taking into account the lattice polarization of a very large crystal region.

Embedding schemes for polar covalent oxides with directional bonds have to face substantial complications due to the necessity that the QM cluster is cut from a covalent framework. Consequently, artificial unsaturated bonds appear for atoms at the boundary of the QM cluster. Therefore, special capping atoms terminating these dangling bonds are introduced in the interface region. For such terminations, H atoms are often used and referred to as "link atoms", with special restrictions for the length and orientation of the saturating bond [26–28]. Since these link atoms are absent in the real system, their energy contributions have to be eliminated [26,27], e.g., by a subtraction scheme as suggested by Morokuma and co-workers for organic compounds and complexes [29]; the approach correctly represents the steric constraints of the framework. Usually in such procedures the QM Hamiltonian does not depend on the charge distribution of the environment and thus effects of the environmental long-range Coulomb potential are accounted for only at classical level. Some approaches have been proposed to overcome this deficiency [28,30,31]. These procedures account for mechanical as well as electrostatic coupling between the QM and classical parts of the system.

3 Electronic structure determination

DFT methods have been developed for the description of crystalline solids (and later of surfaces) and it is only in the last 20 years that they become common practice also in molecular quantum chemistry. It is not surprising that the vast majority of studies done on oxide

surfaces make use of this approach. Nevertheless, there are several issues where a treatment based on wave function methods is desirable. In the following we provide some reasons for this.

3.1 Wave function based methods

The best approximation to the energy of a N-electrons system is given by the Full Configuration Interaction, FCI, approach. However, FCI calculations grow so fast with the number of basis functions that practical computations can be carried out only for systems with small number of electrons. On the opposite side, a simple N-electron wave function can be constructed from a single Slater determinant leading to the Hartree–Fock (HF) approach. Since correlation effects are not included, HF solutions are inadequate for the study of chemical phenomena, including those occurring at surfaces. However, the contribution of the HF determinant to a FCI wave function is by far the dominant term, which means that important qualitative insight in surface and materials chemistry can be and indeed has been obtained in the past from HF calculations [8]. The problem of including correlation effects in an approximate way has been central in quantum chemistry for three decades. This led to the development of various methods like truncated CI methods (e.g. SDCI). Since this requires the diagonalization of very large matrices, it can be used only within the cluster model approach, and are is not very practical for surface studies. Still, examples of SDCI calculations for oxide surfaces have been reported [32]. The alternative based on the estimate of the contribution of the excited determinants by using the perturbation theory (MP2, MP3, MP4, etc.) [33,34] has been used in connection with cluster models. The extension of truncated CI is the so-called Multi Reference CI, MRCI, approach where excitations, usually single and double, from a set of reference determinants are explicitly considered [35]; this approach has been widely used to study optical properties of point defects in silica using cluster calculations [36]. Other ways to solve the correlation problem have been proposed leading to methods like CASPT2 [37,38]. Examples of calculations of optical excitations of surface and bulk defects based on this technique exist [39,40]. The coupled-cluster singles and doubles method with the perturbative estimate of the triples contribution, CCSD(T), is considered to be very accurate for molecular compounds, but its use for surface problems is again very limited because of the very high computational cost. A recent example is that of AuCO complexes formed at the surface of MgO [41].

3.2 Density functional theory based methods

The description of the fundamental aspects of DFT is beyond the scope of this review. However, there are a few points that need to be commented. In DFT the total energy is written as a combination of terms depending on the electron density ρ only:

$$E[\rho] = T_s[\rho] + E_{ext}[\rho] + E_{coulomb}[\rho] + E_{XC}[\rho] \qquad (2)$$

$T_s[\rho]$ is the kinetic energy of the non-interacting electrons, $E_{ext}[\rho]$ accounts for the contribution of the external potential, $E_{coulomb}[\rho]$ corresponds to the classical Coulomb interaction and $E_{XC}[\rho]$ accounts for the exchange part due to the Fermi character of electrons and the correlation contribution. The success of DFT is strongly related to the ability to approximate E_{XC} in a sufficiently accurate way. Once $E_{XC}[\rho]$ is known, the effective potentials are also known and solving the Kohn–Sham equations is similar to solving the HF equation.

Several approaches to $E_{XC}[\rho]$ have been proposed with increasing accuracy and predictive power, starting from the proposal of Vosko et al. [42] known as the Local Density Approximation, LDA, and of its variant for open shell systems Local Spin Density Approximation, LSDA. LDA has been successful in the description of metals, although has experienced more difficulties with ionic solids (for instance, LDA incorrectly predicts a magnetic insulator like NiO to be a metal [43,44]). Being similar to the Unrestricted Hartree–Fock, UHF, formalism, LSDA suffers from the same drawbacks when dealing with open shell systems, in particular in the study of magnetic systems.

The DF methods that go beyond LDA and improve its performances can be grossly classified in Gradient Corrected (GC) or Generalized Gradient Approximation (GGA) and hybrid methods. In the first set the explicit calculation of the $E_{XC}[\rho]$ contributions involves not only the density, ρ, but also its gradient, $\nabla\rho$. The number of GC functionals is steadily increasing but among those widely used for oxide surfaces we quote the Perdew–Wang [45,46], PW, and Perdew–Burke–Ernzerhof [47] exchange–correlation functionals. Another popular gradient corrected exchange-correlation functional is the one proposed by Becke [48], and Lee–Yang–Parr [49], BLYP. Hybrid functionals, a family of methods based on an idea of Becke [50], mix DF and Fock exchange and local and GC correlation functionals in a proportion that is obtained from a fit to experimental data. The most popular hybrid method, B3LYP [50], works surprising well also for ionic and covalent solids despite the fact that the parameters entering the expression of

the exchange functional have been derived on a series of simple molecules.

Before closing this paragraph it is useful to mention that successful examples of applications of DFT to excited state problems have been reported in recent years. This is based on the time-dependent density functional theory (TD-DFT) where excitation energies are calculated from the poles of the frequency-dependent polarizability and the oscillator strengths from the residues. TD-DFT is more accurate than the CI single (CIS) method [51], and can provide transition energies for defects in bulk silica with an accuracy similar to that of MRCI or coupled-cluster methods [52]. However, electronic transitions to states which are close to the conduction band edge are poorly reproduced [52].

3.3 DFT versus wave function methods for solid state problems: open questions

It is still under discussion which functional provides the best chemical accuracy and description of the electronic structure. For many systems this choice is not critical and the use of various functionals permits to add error bars to the computed quantities. However, in the systems of interest in the present review, oxide surfaces and interfaces, the choice of the functional is crucial. We mention here two extreme cases, but the list is longer. The first is the adhesion energy of a metal to an oxide. The case of a Cu atom on the MgO(100) surfaces has been studied in detail [53]. The reported values range from an unbound Cu atom at the HF level to a moderate adsorption, 0.35–0.90 eV, at GC DFT level, to strong adsorption, about 1.5 eV, using LDA. Notice the large spread of gradient-corrected DF values. Ranney et al. [54] have extrapolated the adhesion energy of a single Cu atom on MgO from microcalometric measures of the heat of adsorption, and have found a value of 0.7 eV. This suggests that the BP and BLYP seem to provide the best answer, while hybrid functionals slightly underestimate the adsorption energy [53].

Things are completely different when one considers an extended metal/oxide interface. Mattsson and Jennison [55] have shown that the work of adhesion of Pd(111) to α-Al_2O_3 computed at the LDA level, 2.4 J/m^2, agrees better with the experiment, 2.8 J/m^2 [56], than the GGA adhesion energy, 1.6 J/m^2 . This is quite surprising in view of the superior performances of GGA for energetics. The interfacial bonding of Pd(111) to a wide-gap ionic oxide (like MgO or α-Al_2O_3) is dominated by local polarization contributions which are well described by DFT, but the surface energies of both the metal and the oxide have substantial errors due to self-interaction. The correction is much larger for GGA than for LDA, where an accidental cancellation of errors produces better agreement with experiment. Once the surface energies have been corrected, e.g. following a scheme recently proposed by Mattsson and Kohn [57], both the GGA and LDA adhesion energies are within the experimental error bars. The last word about the method of choice in the calculation of adhesion energies of metal overlayers to oxides has not yet been written.

The other example is related to the description of spin properties, such as the EPR spectra of trapped electrons or of paramagnetic defects, the magnetic coupling of transition metal ions, etc. The "classical" model of an $[AlO_4]^0$ defect center in quartz, an Al impurity replacing a four-coordinated Si atom, is that a hole forms on a non-bonding orbital of an O atom with consequent asymmetric relaxation along one particular Al-O direction. This model has been proposed several years ago based on the analysis of the EPR spectra of Al-doped SiO_2 [58] and of HF cluster model calculations [59]. Theoretical studies based on DFT (LDA or GGA) and supercell plane wave calculations proposed an alternative model where the hole is completely delocalized over four O neighbors to the Al impurity [60,61]. From the direct comparison of computed and measured hyperfine and superhyperfine coupling constants it follows that this latter picture is incorrect [15]. The different physical description emerging from cluster HF and supercell DFT calculations has nothing to do with the model used, cluster or supercell, but is due to the non exact treatment of exchange in DFT and to the well known problem of the self-interaction correction. Care is needed when DFT is used to describe localized holes in insulators [15].

In general, the treatment of materials like magnetic insulators, oxides of the f-elements or similar compounds characterized by the presence of partially filled d or f shells, requires the use of hybrid functionals or, in alternative, of the LDA+U or GGA+U methods. This latter approach was proposed by Anisimov et al. [62] to bridge the gap between conventional LSDA methods and the Hubbard model. The DFT+U method provides an alternative to correlated cluster-based calculations. The solid is treated as a periodic continuum and on-site electron repulsion terms are included using an effective one-electron potential which acts differently on the occupied and unoccupied orbitals. Also the size of the band gap in insulators, an important property in the context of oxide surfaces, is better described at the DFT+U level, although it has been shown that hybrid functionals like the B3LYP approach provide very accurate predictions of this quantity [63]. For all these reasons new algorithms have been recently developed aimed at introducing hybrid functionals also in connection with plane wave approaches [64].

4 Structure and properties of oxide surfaces

The chemistry of oxide surfaces depends basically on four main factors: (1) nature of the bonding (ionic, covalent, or semi-covalent) and electronic structure of the oxide (wide gap insulator, semiconductor, or metallic); (2) surface morphology (nature and abundance of low-coordinated sites, presence of extended defects, surface area, porosity, etc.); (3) functionalization (doping with heteroatoms, electron rich surfaces, mechanically activated surfaces, etc.); (4) redox properties (reducible transition metal oxides, presence of partially filled d or f shells, etc.). The identification of the importance of each of these terms is a typical task for theory. In the following we provide a number of examples which illustrate how surface chemistry of oxides depends on these aspects.

4.1 Ionic bonding in oxides and surface chemistry: the example of H adsorption

A good example of reactivity of an oxide surface related to the bonding nature in the material is the reaction with H atoms. Different oxides give rise to completely different behaviour in this respect. Let us consider alkaline-earth oxides and in particular MgO, a prototype of ionic oxides with NaCl-type structure and a morphology based on extended (100) planar faces where both Mg^{2+} and O^{2-} ions are five-coordinated (5c) and chemically inert. Depending on the preparative method, surface areas of up to 1,000 m^2 g^{-1} can be produced [65]. As a result, low-coordinated ions, primarily located at the steps or edges (four coordinated, 4c), kinks or corners (3c), etc., become more abundant. Exposure of MgO [66] or CaO [67] powders to H atoms results in the formation of excess electrons which are responsible for the blue color acquired by the material. EPR spectroscopy shows that paramagnetic centers are formed on the surface. For many years it has been assumed that H atoms split in a trapped electron, (e^-), and a proton, (H^+), by reaction with specific point defects like the F_s^{2+} centers, electron deficient oxygen vacancies (see Sect. 4.2) [68]. The difficulty to reconcile some experimental evidence with theoretical models lead to the suggestion of a different possibility, i.e. that the H atom is ionized by "normal" Mg and O ions on the surface due to the strong electrostatic potential generated by the ionic oxide [69,70]. This reaction does not occur on the surface of other oxides like, for instance, SiO_2. On MgO the splitting of the H atom in a proton (H^+) adsorbed on a O^{2-} anion and an electron (e^-) trapped near one or more Mg^{2+} cations occurs *only* on low-coordinated sites with an exothermic reaction, Fig. 2. The resulting paramagnetic center, named $(H^+)(e^-)$ pair, can be obtained

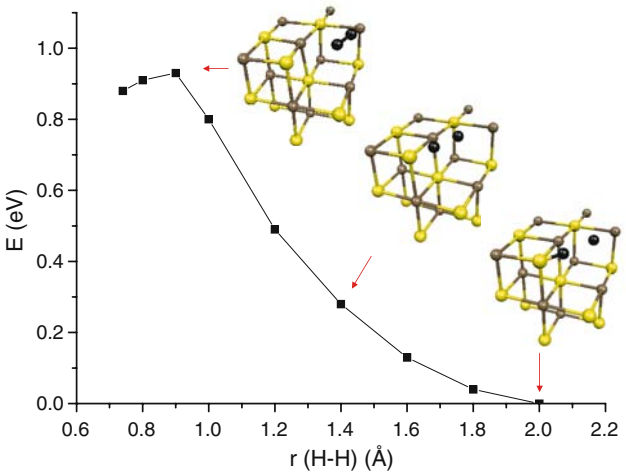

Fig. 2 Potential energy curve for the dissociation of an H_2 molecule on a reverse corner site of the MgO surface. The dissociation has a small activation barrier and leads to the formation of (H^+) and (H^-) ions bounds to O anions and Mg cations, respectively. The corresponding reaction is exothermic

by heterolytic dissociation of H_2, Fig. 2, followed by UV irradiation, and exhibits computed EPR hyperfine coupling constants, O–H vibrations, and optical transitions, in complete agreement with the experimental data [69,71,72]. The chemical process, which occurs at temperatures as low as 77 K, is

$$Mg^{2+}{}_nO^{2-} + H^\bullet \rightarrow Mg^{2+}{}_n(e^-)(O^{2-}H^+) \quad (3)$$

and leads to the formation of electron-rich alkaline-earth metal oxide surfaces. Notice that this reaction does not take place on flat (100) terraces, nor in the bulk. Thus, by exposing nanostructured polycrystalline alkaline-earth oxides to H atoms (or to H_2 molecules under UV light) one has a way of "dropping" excess electrons on specific surface sites.

This has important consequences on the surface reactivity. Molecules exposed to electron-rich surfaces are irreversibly reduced, via electron transfer, to the corresponding radical anions. Here the ionic surface acts both as reducing agent and stabilizing medium. Many examples of this reactivity have been studied over the years. Molecular oxygen readily reacts with $(H^+)(e^-)$ surface pairs to form the superoxide O_2^- radical ion which is then stabilized in proximity to the adsorbed proton (hydroxyl group) [73,74]:

$$O_{2(gas)} + (H^+)(e^-)_{surf} \rightarrow (O_2^-)(H^+)_{surf} \quad (4)$$

Ab initio calculations provided essential information for the identification of the resulting radical species, mainly based on the comparison of calculated and measured ^{17}O hyperfine coupling constants [75]. Surprisingly, also N_2 interacts with $(H^+)(e^-)$ centers below 100 K with

formation of a N_2^- surface radical, with a net one electron transfer from the surface to the N_2 π^* orbitals [76,77]:

$$N_{2(gas)} + (H^+)(e^-)_{surf} \rightarrow (N_2^-)(H^+)_{surf} \quad (5)$$

The bond of the activated N_2^- molecule is ~9% longer in the reduced state. This is a rare example of formation of N_2^- radical anion on a surface, with a completely reversible process. The reversibility has been explained by quantum chemical calculations, which identified a very small energy barrier between the N_2^-/MgO bound state (electron transfer) and the N_2/MgO physisorbed state [76,77].

The interaction of atomic hydrogen with covalent oxides like SiO_2 or transition metal oxides like TiO_2 is completely different from that of MgO. Periodic DFT calculations [78] and EPR measurements [79] show that in bulk silica or on the silica surface the H atom interacts very weakly with the pores of the material and that therefore posses high mobility even at temperatures as low as 30 K [80]. Only with specific point defects (e.g. oxygen vacancies) the neutral H atom interacts chemically to form stable complexes [78]. The reason is that the silica regular lattice is held together by strong covalent bonds which do not exhibit any tendency to react with the H radical. Hydrogen atoms do not reduce the SiO_2 lattice. This is opposite to TiO_2. Here the addition of an H atom to the bridging oxygens of the rutile (110) surface results in the formation of a proton bound to the O site (hydroxyl group) and one electron which is accommodated in the 3d states of a nearby Ti ion ($Ti^{4+} \rightarrow Ti^{3+}$). As a consequence, a reduction of the surface occurs with similar characteristics of an oxygen deficient TiO_2 surface [81]. The properties of the H-reduced TiO_2 surface have been recently discussed based on periodic DFT calculations. It was shown that the inclusion of the exact Fock exchange (e.g. using the B3LYP hybrid functional) is essential for the correct description of the hydroxilated surface [81].

4.2 Surface defects and morphology: where reactions occur

Many properties of inorganic materials and of their surfaces are controlled, beside their geometric and electronic structure, by faults or defects in the structure [82,83]. Defects are terribly important in chemistry, as they largely determine phenomena like corrosion and catalysis by certain oxides. The chemical, electrical and optical properties of bulk defects have attracted a continuously increasing interest in material science, to the point that a new discipline, defect engineering, has emerged. Defect engineering is aimed at manipulating the nature and the concentration of defects in a material so as to tune its properties in a desired manner. While this is well known in the field of bulk materials, it is only recently that attention has been given to the problem of defects at oxide surfaces.

Just to give an example, about a dozen of different types of defects and irregularities has been identified and described in the literature for MgO [84]. Appreciable concentrations of defects can change completely the chemical behavior of the MgO surface. For instance, while a single crystal nearly defect-free (100) MgO surface is totally inert towards CO adsorption [85], polycrystalline MgO reacts at low temperature with the same molecule with formation of complex carbonate species [86] (see also Sect. 4.2).

Among the defects identified at oxide surfaces the oxygen vacancy has attracted the greatest attention. Depending on the material, the structure and properties of oxygen vacancies can vary substantially to the point that they can be considered as a fingerprint of the electronic structure of the oxide. Let us consider two simple binary oxides like MgO and SiO_2. In MgO a missing O atom from the bulk or from the surface results in two trapped electrons localized in the cavity center, Fig. 3a. The driving force for the electron localization is the Madelung potential of the highly ionic crystal. The

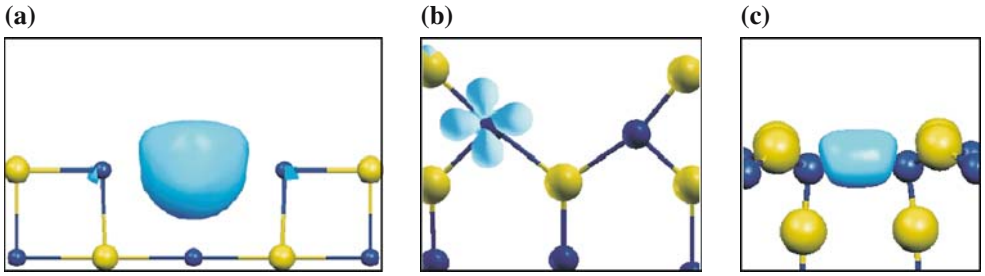

Fig. 3 Charge density plots for an oxygen vacancy created on **a** an ionic crystal (e.g. MgO), **b** a transition metal oxide (e.g. TiO_2), and **c** a covalent-polar oxide (e.g. SiO_2). In **a** two electrons are trapped at the center of the cavity by strong electrostatic potential of the ionic lattice; in **b** the electrons are localized on atomic-like d orbitals of the transition metal cation; in **c** the two electrons occupy a bonding orbital with formation of a direct bond between the two cations (e.g. a Si–Si bond)

place occupied by O^{2-} in the regular lattice is taken by two "free" electrons in the defective crystal, so that the removal of a neutral O atom from the MgO surface results in a very small local relaxation (less than 1%). The electrons trapped at an oxygen vacancy in MgO give rise to new states in the gap of the material and to typical excitations in the visible region of the spectrum, thus changing the color of the defective material (these centers are called F centers, from Farbe, the German word for color). The position of the impurity levels associated to F and F^+ centers generated by electron bombardment on MgO/Ag(100) films has been established by scanning tunneling spectroscopy (STS) and interpreted from cluster model calculations [87].

The situation is completely different in SiO_2, a solid characterized by covalent polar bonds. In SiO_2 the removal of an O atom from a ≡Si–O–Si≡ linkage results in two Si dangling bonds, ≡Si•, which recombine to form a ≡Si–Si≡ covalent bond with two electrons occupying a localized Si–Si bonding state, Fig. 3c [88]. The process is accompanied by a strong geometrical relaxation (the Si–Si distance decreases from 3.06 Å in the regular lattice to 2.4–2.5 Å) and the associated optical transition involves localized excitations from a bonding to an antibonding state in the gap [88]. The nature of the oxygen vacancy in the two oxides, therefore, is completely different as the result of the different electronic structure, highly ionic in MgO, covalent polar in SiO_2.

What about intermediate cases like the surface of TiO_2, a reducible transition metal (TM) oxide? TiO_2 has a ionicity intermediate between fully ionic (Ti^{4+} and O^{2-}) and covalent; a rough estimate indicates a charge of about +2 on Ti and −1 on O [89]. The presence of d orbitals on Ti offers new possibilities to redistribute the electrons involved in the bonding with the O atom which has been removed. A characteristic of TM metal oxides is the possibility to change the oxidation state of the metal. The creation of an O vacancy in TiO_2 leads to a situation which differs from those described above for MgO and SiO_2. In TiO_2 in fact, the two electrons associated to the vacancy are neither trapped in the cavity (as in MgO) nor lead to the formation of a Ti–Ti bond (as in SiO_2). Rather, they are transferred to the empty 3d levels at the bottom of the conduction band belonging to the adjacent Ti atoms, Fig. 3b and Fig. 4 [90]. Since the 3d states are rather localized, this corresponds to a change of the formal oxidation state, from Ti^{+4} to Ti^{+3}. The presence of an unpaired electron in the 3d shell of the Ti atom leads to the formation of a paramagnetic defect [90].

This is an important characteristic of a defect. In fact, defects are often elusive species, highly diluted, and difficult to detect. Often the proofs of their existence are

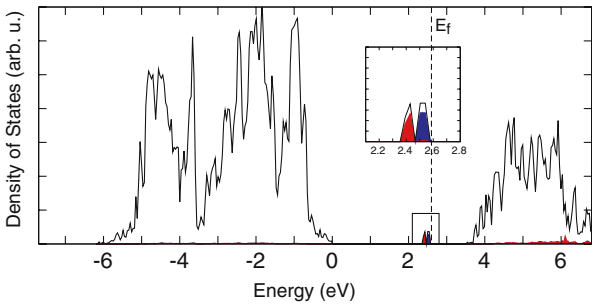

Fig. 4 Density of states (DOS) of an oxygen vacancy in TiO_2 as obtained from a B3LYP periodic calculation. The DOS shows the presence of occupied states in the gap of the semiconductor oxide, at about 1 eV below the conduction band

indirect, based on the change of a property or of a spectroscopic response as a function of the defects concentration. When defects consist of single electrons trapped in special sites they can be detected by EPR. This technique is rather sensitive, being able to reveal 10^{12} spins; this means that for a high surface area polycrystalline sample of, say, 200 m^2 /g the lower limit of sensitivity is of 10^7 spins/cm^2, i.e. about a paramagnetic center every 10^8 surface atoms. This is much better than the sensitivity of optical measurements which, for high dilutions, cannot detect the electronic states associated to the defect.

We consider now the activity of another kind of defect, the low-coordinated sites. We do this by analyzing the adsorption properties of CO [91–93]. As we mentioned before, the (100) surface of MgO, where all the ions are 5c, is unreactive towards CO which binds very weakly at the cation sites (by 0.13 eV) [85,94,95]; thus, CO sticks on the (100) surface only at temperatures well below liquid nitrogen. Ultra-thin MgO films [4,96] exhibit similar properties to those of MgO single crystal surfaces provided that the morphology of the films is well controlled. In fact, CO binds to low-coordinated Mg^{2+} cations at steps or corners with energies of 0.2–0.4 eV [97,98], and a direct correlation exists between the strength of the Mg–CO bond and the C–O stretching frequency which is shifted to higher values by effect of the field-dipole interaction [99–101]. This allows one to detect and titrate low-coordinated cation sites on high-surface area MgO samples [91].

Even a rather unreactive molecule like CO interacts with the exposed oxide anions of MgO located at edges, steps, corners, to form complex anionic polymeric species [93]. This occurs at low-temperature and has been followed by infra-red (IR) spectroscopy [91]. Low-coordinated oxide anions of MgO exhibit a large basicity [102]. This has been rationalized in terms of reduced Madelung potential, U_{Mad}, at exposed sites of an ionic surface [103]. The O^{2-} ion is unstable in gas-phase where it dissociates spontaneously into $O^- + e^-$, but exists in

ionic oxides because of the stabilizing effect of U_{Mad}. However, U_{Mad} decreases going from the bulk (6c) to the surface (5c) and even more to steps, edges, corners and kinks (3c or 4c) [13]. A lower U_{Mad} shifts to higher energies the filled O 2p levels of the O^{2-} ion, and increases their basic character [103]. In fact, this destabilization favors the transfer of charge to an acceptor molecule that binds to this site. Still, the high reactivity of low-coordinated oxide anions of MgO is surprising in view of the complete absence of reactivity of the same ions placed on regular terraces.

DFT calculations have permitted to unravel interaction mechanism, structure, and properties of the $(C_nO_{n+1})^{2-}$ polymeric species that form on MgO nanocrystals [104]. Oxide anions at steps, edges, kinks, corners form with CO complex polymeric species, $[O_{lc}(CO)_n]^{2-}$ ($n = 1$ to 5), see Fig. 5, with exothermic, non-activated reactions, thus explaining the high reactivity even at very low temperatures. The calculation of the vibrational properties has allowed a direct comparison with the measured IR spectra, leading to the conclusion that the first sites reacting with CO are the 3c oxide anions at corners (or kinks); only at higher CO exposures also the step and edge sites adsorb CO, probably after all the 3c sites have been populated [104].

The very different reactivity of oxide anions located on different sites of the MgO surface is a clear example of the importance of the morphology in determining the properties of oxide surfaces. Both statements "MgO is *completely unreactive* towards CO" and "MgO is *very reactive* towards CO" are correct, despite they contain contradictory messages. The reason is that when discussing oxides reactivity, it is not sufficient to mention the oxide, but one has to specify its form (single crystal, polycrystalline, amorphous, thin film, etc.) and morphology. Today, a large effort is directed to the preparation of nano-structured oxide materials with properties that differ substantially from those of the corresponding "classical" forms.

4.3 Doping and functionalization of oxide surfaces

Intrinsically unreactive oxide surfaces can become reactive by inclusion of heteroatoms diluted in the oxide matrix, by anchoring adsorbed molecules, etc. This process, known as functionalization, is very important in the preparation of materials with new properties. Even the tailored creation of specific defects can provide a way to modify the surface chemistry (see Sect. 4.2). One example of functionalization reported in the following is that of Ni ions introduced in the MgO matrix and their role in N_2O decomposition.

The decomposition of N_2O over oxide surfaces has been studied intensively because of the environmental

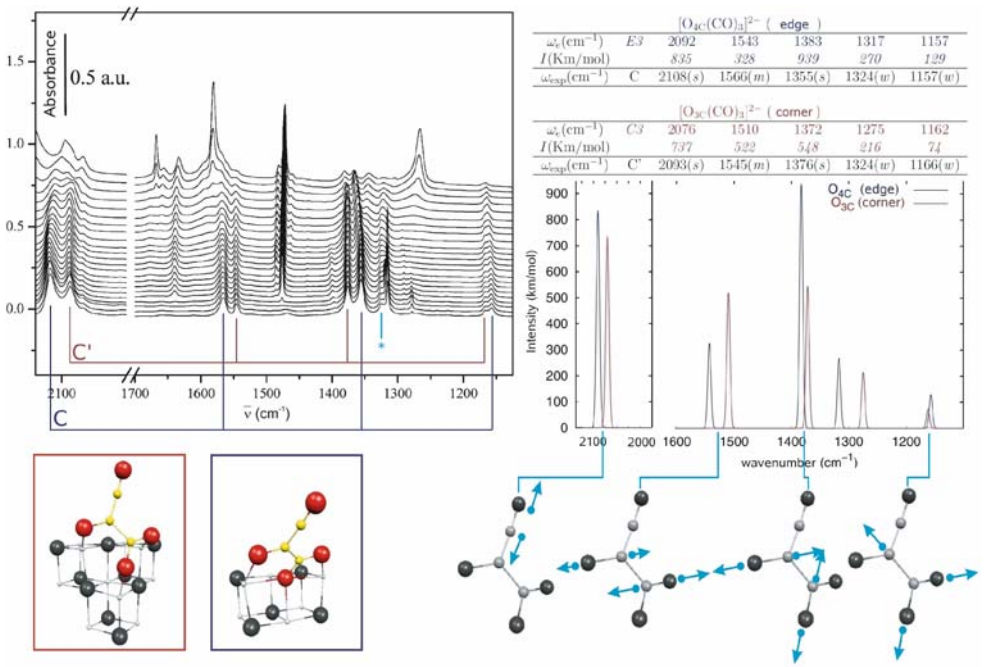

Fig. 5 The figure shows the experimental IR spectrum of CO adsorbed on polycrystalline MgO (*left*) and the simulated spectrum (*right*, see also corresponding values in the two tables and normal modes in the *inset*). The data reported refer to $O_{4c} - (CO)_3^{2-}$ and $O_{3c} - (CO)_3^{2-}$ trimers formed at 4c (edge) and 3c (corner) oxide anions of the MgO surface (see inset on the *left*). Reprinted from [104]

problems connected with the release of this molecule in industrial processes or from car exhausts [105,106]. One of the systems which has been studied most is MgO. It has been suggested [106] that the dissociative reaction of N_2O follows a Eley-Rideal mechanism in which the oxygen atom of N_2O is transferred to the surface O^{2-} anion with formation of a peroxo group, O_2^{2-}:

$$N_2O_{gas} + O^{2-}_{surf} \rightarrow N_{2gas} \uparrow + O^{2-}_{2surf} \quad (6)$$

The reaction then proceeds by recombining two oxygen atoms and desorption of an O_2 molecule:

$$2O^{2-}_{2surf} \rightarrow O_{2gas} \uparrow + 2O^{2-}_{surf} \quad (7)$$

The formation rate of N_2 and O_2 per surface area increases linearly with the inclusion of Ni ions in a MgO matrix, reaching a maximum for a Ni concentration of about 50% [107]. With this material the activity is 20 times higher than on pure MgO. Thus, the presence of Ni at the catalyst surface is essential for increased N_2O decomposition. The role of Ni impurities in Ni-doped MgO has been investigated theoretically with cluster models [108]. The oxygen abstraction from N_2O is the rate limiting step and the computed barrier, 1.37 eV for MgO terrace and 1.34 eV for MgO edge sites, is very close to that determined experimentally, 1.3 eV [109]. On the Ni-doped surface the nature of the transition state is the same as for pure MgO, but the barrier is reduced by about 0.2 eV, sufficient to explain the increase in rate of formation of N_2 by about one order of magnitude with respect to pure MgO [107]. This shows how the dilution of a small amount of extra atoms in the oxide structure is sufficient to deeply modify the surface activity.

4.4 Redox properties of transition metal oxide surfaces

Compared to MgO or SiO_2, TM oxides offer a much richer chemistry largely related to their redox properties. TM metal oxides are often non-stoichiometric, can change composition and oxidation state of the metal cation, and span a broad range of properties (ferroelectric, paraelectric, magnetic, etc.). Here we discuss a special case of surface reactivity connected to redox properties of titania.

The adsorption of Au atoms, clusters and particles on TiO_2 surfaces is without any doubt the most intensively studied problem in the field of supported metal clusters on oxides under controlled conditions [110–115] (see also Sect. 6). This is stimulated by the not yet resolved problem of the catalytic CO oxidation promoted by small Au particles deposited on titania discovered by Haruta some years ago [116]. In a recent study Au atoms have been deposited on reduced and oxidized TiO_2 thin films grown on Mo(110) in UHV [117]. DFT plane wave calculations have shown that Au forms a weak bonding to the regular surface, $D_e < 0.5$ eV, and that keeps the $5d^{10}\ 6s^1$ atomic configuration. Little or no charge transfer occurs between Au and the surface [117]. Things change dramatically on O vacancies, quite abundant on TiO_2 and characterized by the presence of two reduced Ti^{3+} atoms near the vacancy (see Fig. 4 and Sect. 4.2). On these defect sites Au is bound by ≈1.8 eV [117]. Spin density plots show that the spin is localized inside TiO_2 and that no spin density is left on the Au atom (closed shell). The analysis of the density of states (DOS) shows that the 6s level of Au is filled and falls below the Fermi level, Fig. 6. Thus, the Au atom bound to an O vacancy of TiO_2 is formally $5d^{10}\ 6s^2$ and can be viewed as Au^- anion (notice that gold has a high EA, 2.31 eV according to both experiment and calculations). This is a clear example where the reduced TiO_2 surface acts as an *electron donor*, and is able to reduce the adsorbed Au species. Next we show that the opposite mechanism, i.e. the transfer of electrons from the adsorbate to TiO_2, is also possible.

A CO probe molecule has been adsorbed on the supported Au atoms to check the nature of the Au–TiO_2 interaction. On stoichiometric TiO_2 neutral Au atoms are preferentially bound to the bridging oxygens of the surface. When a CO molecule is added, a strong change in the Au-support interaction occurs: the 6s electron of Au is transferred to the Ti 3d states, Au becomes formally Au^+ and the TiO_2 substrate is reduced! The Pauli repulsion with the CO 5σ orbital destabilizes the 6s level of Au which is pushed above the Fermi level; the 6s electron is transferred to the substrate and almost no spin density is left on gold. In this way the CO molecule can

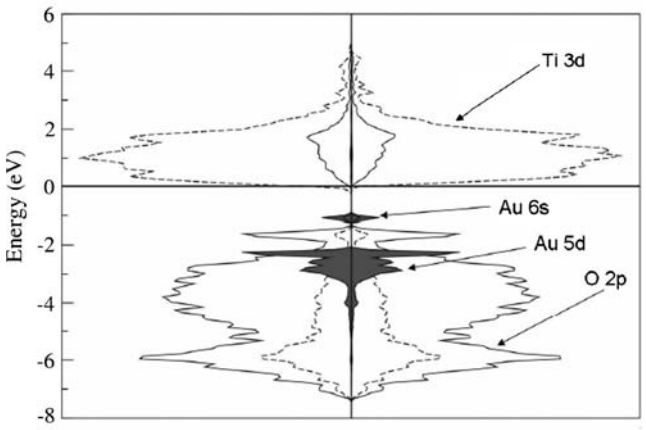

Fig. 6 Density of states of an Au atom adsorbed on an oxygen vacancy of the rutile $TiO_2(110)$ surface

form a strong bond with Au, 2.4 eV, close to that of gas-phase Au^+ –CO, 2.08± 0.15 eV [118]. The Au → TiO_2 charge transfer is demonstrated also by a blue-shift in the CO vibrational frequency typical of CO adsorbed on metal cations, from 2,097 cm^{-1} of gas-phase AuCO to 2,151 cm^{-1} of TiO_2 supported AuCO. The agreement between computed and measured CO stretching frequencies for AuCO complexes formed on reduced and oxidized TiO_2 surfaces provides a solid verification of the theoretical predictions [117].

This is a clear example of how TM oxide surfaces can act both as reducing agents (in this case the activity is related to the presence of defects), or as oxidizing species. It also shows an example where CO does not act simply as a probe molecule but induces a strong change in the adsorbate (Au is neutral before CO adsorption, and positively charged after). In Sect. 6.1 we will see another example where CO does not simply act as a probe molecule, but on a different substrate, MgO.

5 Thin oxide films on metal substrates

Thin oxide films epitaxially grown on metal substrates constitute a class of materials with unprecedented properties and potential applications in magnetic tunnel junctions, dielectrics in miniaturized electronic devices, plasma display panels, supports for metal nano-catalysts, etc. It is possible to tune their electronic properties by changing the oxide film thickness or the metal support, thus changing the interface bonding, film structure, lattice parameter, etc. In the last 15 years an intense activity has been directed to the preparation and characterization of these systems [4,119]. So far, the attention has been mostly on film structure (often this differs from the bulk one), on chemical properties (relationship between surface morphology, defects and chemical reactivity), or on the possibility to deposit in a controlled way metal nano-clusters and even isolated atoms. However, oxide films induce other important modifications in the electronic structure of the system, in particular they can lead to a significant increase or decrease of the work function of the metal substrate, Φ_{met}.

One of the consequences is that the deposition of nano-clusters on the oxide surface can result in a charge transfer to or from the substrate depending on the position of the corresponding Fermi energies [120]. The charge transfer can spontaneously occur through tunneling mechanisms or can be stimulated by an external electric field like that of an STM tip [121]. A peculiar behavior of Au atoms on MgO/Mo(100) or MgO/Ag(100) ultra-thin films has been predicted theoretically [120,122]. In particular, Au atoms become Au^- anions by capturing an electron from the Mo conduction band via electron tunneling through the thin dielectric barrier. Recent experiments on Au atoms deposited on Al_2O_3/NiAl(110) and on MgO/Ag(100) films seem to support this view [123]. This phenomenon can lead in principle to a new class of materials where the charge state (positive or negative) of a deposited metal nanoparticle is determined by the nature of the metal/oxide interface.

To better illustrate this concept let us consider four interfaces, MgO/Ag(100), MgO/Mo(100), TiO_2/Mo(100) and SiO_2/Mo(112) (for a detailed description of the structure of these films see below Sect. 6.1) [124]. DFT plane wave calculations have shown that MgO films induce a decrease of Φ of 1–2 eV compared to the metal substrate, Fig. 7 (Φ goes from about 4 eV to less than 3 eV). A recent experimental estimate of ΔΦ for MgO/Mo(100) is about −1 eV; on W(110) ΔΦ is −1.8 eV [125]. Both sign and magnitude of these shifts are consistent with the theoretical predictions. SiO_2 and TiO_2, on the contrary, induce an increase of Φ of about 0.5–1 eV. Work function measurements for SiO_2/Mo(112) give an estimate of 5.2 eV, 0.8 eV more than for the free metal [126]. On TiO_2/Mo(100) films the increase in Φ is of 0.5 eV [125]. These values are in qualitative agreement with the DFT calculations. In particular, notice the different sign of the work function change going from MgO to SiO_2 or TiO_2 films, which reflects the different bonding at the interface.

The shifts in work function have a different origin for the various oxides considered. For SiO_2 and TiO_2 the increase in Φ can be explained with the classical model

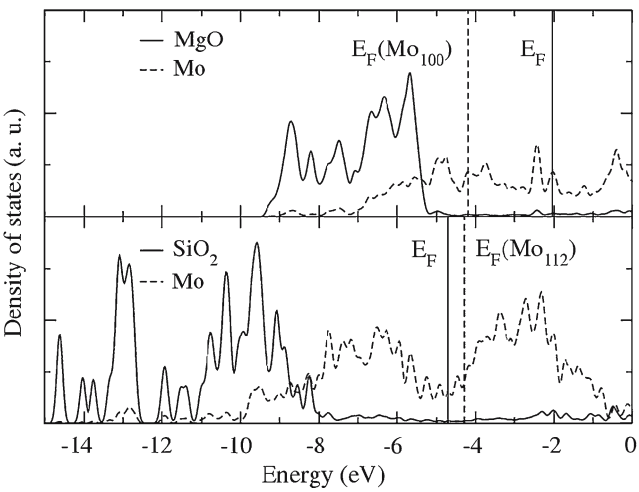

Fig. 7 Projected density of states of MgO(3L)/Mo(100) (top) and SiO_2/Mo(112) (bottom) supported films. The vertical solid line indicates the position of the Fermi level (taken here as a measure of the surface work function) in the metal/oxide system; the vertical dotted line indicates the position of the Fermi level in the pure metal substrate

of surface dipole due to metal-to-oxide charge transfer at the interface. On the contrary, MgO/metal interfaces exhibit a negligible charge transfer from the oxide to the metal, by far too low to justify the large changes observed. The change in Φ is due to a polarization of the metal electron density enforced by the oxide layer, with consequent change in surface dipole [124]. These results show that this property can be tuned and modified in metal/oxide interfaces, an important aspect for the design of new materials based on ultra-thin oxide films.

6 Supported metal clusters on oxides

There are several reasons why supported metal clusters can play a role in nanoscience and nanotechnology [1,2,7,127,128]. The most immediate application is related to catalysis by supported metal particles [6]. In order to be active, the metal particle must have a size of a few nanometers. The better is the control on the size distribution of the particles, the more efficient is the catalyst. However, despite several efforts to better characterize the relationships between surface morphology, size, and shape of the metal particles, a deep understanding of the catalytic mechanisms if often lacking. Nanocatalysis is a field related to the possibility to produce new catalysts at the nanoscale under controlled conditions. Other fields where supported metal clusters will play a role are in the microelectronic technologies and in particular in the production of sensors, in magnetic recording, or in optoelectronic applications.

6.1 Metal atoms on oxides

Nowadays it is possible to prepare in a controlled way assemblies of atoms on "inert" supports and manipulate them at the atomic scale. Examples of chemistry on single metal atoms have been reported [5,129–132], showing also that modifications of the chemical activity are possible by stabilizing the metal atoms at specific defects of the surface [129]. This opens stimulating perspectives in the field of nanotechnology. One general problem is the characterization of the electronic properties of the supported metal atoms. Indirect information can be obtained from adsorption of CO molecules and from the measurement of their vibrational shift, but some care is required in the interpretation of the results. We have seen above that CO can induce deep changes in supported ad-atoms, as in the case of TiO_2 where it induces a charge transfer from Au to TiO_2 (see Sect. 4.4). Another example in this direction is that of CO adsorbed on Au atoms supported on MgO(100) [133]. While a Au atom on MgO is neutral, the addition of CO leads to a charge transfer from the oxide to the AuCO complex, which formally becomes $[AuCO]^-$, with consequent huge red-shift of nearly 300 cm^{-1} in the CO stretching frequency which becomes $\cong$1,850 cm^{-1}. This result has been obtained, beside very accurate experiments, with a variety of computational methods, from plane wave DFT with ultra-soft pseudopotentials to fully relativistic all electron DFT calculations, from B3LYP to CCSD(T) using cluster models, etc. [41]. It shows that the predictive level of theory in this field is similar to that reached in the more classical area of molecular chemistry.

EPR is a powerful technique to study paramagnetic adsorbed atoms. It has been used on polycrystalline high-surface area MgO to identify the properties of adsorbed alkali metal atoms [67,68,134]. K atoms are stabilized at specific morphological sites of MgO, the reverse corners, where they are stable up to 380 K [135]. Above this temperature diffusion and aggregation processes take place. The MgO surface acts as a kind of "solvent" which perturbs the spin properties of the adsorbed K atom, and its hyperfine coupling constants (hfcc) deviate strongly from that of the free atom. In particular, the isotropic constant, a_{iso}, is reduced by 50% when K is adsorbed on a reverse corner [135], despite the fact that no charge transfer occur. EPR measurements are considerably more difficult to perform under UHV conditions. Here the advantage is the atomistic control of the surface morphology thanks to the use of STM for the characterization of ultra-thin oxide films [136]. The price to pay, however, is a considerable loss in EPR signal intensity as the surface area at disposal is strongly reduced, from hundreds of m^2 /g of powder samples, to 1–2 cm^2 in the thin film regime. The detection limit of EPR equipment is sufficient to collect well resolved EPR spectra for paramagnetic atoms adsorbed on thin MgO/Mo(100) films [136]. The study of deposited Au atoms at very low temperature (30 K) has unambiguously shown adsorption on-top of O anions of the MgO(100) terraces [136]. Changes of the order of 50% have been observed in the a_{iso} value of the adsorbed Au atom in analogy with the results for K on MgO powders [135], despite the different adsorption sites (flat terraces for Au and reverse corners for K). These experimental studies have opened various questions for theory. In fact, the EPR properties of atoms such as K and Au are very sensitive probes for the interaction with different surface sites (notice that while the calculation of hyperfine properties of K atoms can be done with standard all electron approaches, the study of Au requires to perform all electron fully relativistic calculations [137]). The large reduction of a_{iso}(Au) or a_{iso}(K) when the atoms

are deposited on MgO is not related to the occurrence of charge transfer or to s–p hybridization of the atoms. Rather, it is due to an expansion of the outer s electron to reduce the Pauli repulsion with the surface. DFT has been able to reproduce in a satisfactory way both the hyperfine and superhyperfine constants (with the ^{17}O isotope), although for Au the errors are larger due to inherent approximations in the relativistic approach [135,136].

As a second example of adsorbed metal atoms on oxide surfaces we consider that of Au and Pd on SiO_2 [138]. Metal atoms deposition has been studied in detail on MgO, Al_2O_3, and TiO_2, but only in the last years an intense effort has been directed towards silica. The reason is that the silica surface is often disordered, defect-rich, and difficult to characterize. Thin silica films, well known for their use in the microelectronic industry, grow amorphous on Mo(110) and Mo(100) substrates [139] and only recently well-ordered crystalline silica films have been prepared on Mo(112) [140]. The film consists of a single silica layer of 3–4 Å thickness, formed by SiO_4 tetrahedra which share three Si–O–Si bridges with the forth oxygen directly bound to the Mo substrate, Fig. 8 [141,142]. The elucidation of the structure of the SiO_2/Mo(112) films, based on combined DFT calculations, and FT-IR, STM, and LEED measurements [141,142], has opened new perspectives for the theoretical modeling of deposited atoms like Au and Pd.

According to plane wave DFT calculations, both deposited Au and Pd atoms interact weakly with the regular Si or O sites of the SiO_2 surface ($D_e < 0.3$ eV) [138].

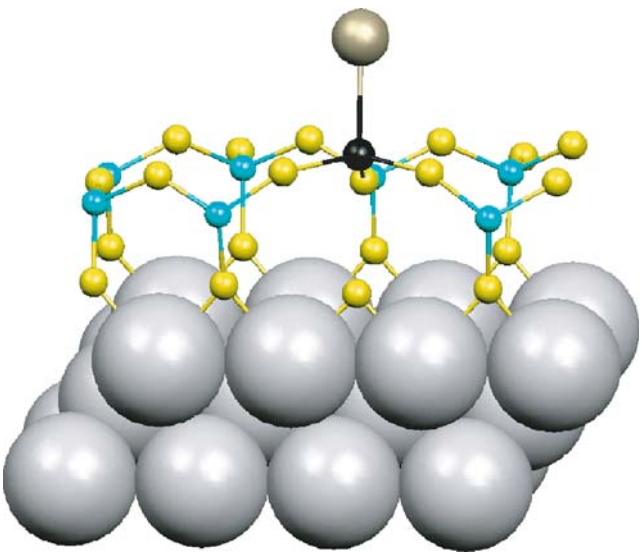

Fig. 8 Structure of an adsorbed Au atom on a $Ti_xSi_{1-x}O_2$/Mo(112) film (side view). *Pale blue atoms* Si; *yellow atoms* oxygen; *black atom* titanium; *gray atoms* Mo

Fast diffusion of the deposited atoms is thus expected even at very low temperatures. Because of the smaller dimensions, however, Pd can bind more efficiently than Au to the silica rings, partially interacting with the SiO_2/Mo interface. These theoretical results have been used to rationalize the observed growth of small metal particles on SiO_2/Mo(112) films. Generally, two major kinds of defects are expected to be present in these films: extended defects like steps and domain boundaries, and point defects, most likely oxygen vacancies. Deposition of Au at RT on a film low in point defects results in the preferential nucleation and grow of the Au clusters on the extended defects [143,144]. On the contrary, when a SiO_2 film with a high density of point defects is prepared, the clusters nucleate and grow in correspondence of the point defects on the terraces [143,144], a result which is fully consistent with DFT calculations [138]. A different behavior is expected for Pd. Since the Pd atom can bind more efficiently with the six-member rings of the silica terraces, Pd clusters on the silica film will produce homogeneous nucleation even on defect-poor films. In fact, the Pd atom bound at the SiO_2-Mo interface can start the nucleation of a small cluster. This is consistent with the observation that at Pd nanoclusters exist randomly on the terraces of the on SiO_2/Mo(112) film [145], at variance with Au where decoration of the line defects is observed [143,144].

Quite different is the behavior of Ti-doped silica films. Recent studies by Goodman et al. [143,144] have shown that the propensity of the silica films to bind and stabilize deposited metal atoms grows significantly by doping the films with Ti. Highly diluted Ti atoms replace Si in the film without significant structural or electronic changes: they remain tetrahedrally coordinated, and formally keep a +IV oxidation state [138]. However, the Ti impurities introduce low-lying empty levels with Ti 3d character in the silica gap. These states can easily hybridize with the orbitals of the adsorbed Au and Pd atoms, induce substantial surface reconstruction, Fig. 8, and form relatively strong bonds. These results shed light into the mechanism of nucleation and growth of small Au clusters on Ti-doped silica films [143,144]. In fact, STM images show that gold clusters form in correspondence of the protrusions due to the Ti defects [143,144]. This is another example of functionalisation of an oxide surface (see Sect. 4.3) which could also be important to enhance the catalytic properties of the Au/SiO_2 system.

6.2 Growth of supported of metal clusters on oxides from self-assembly of isolated atoms

Two different approaches are usually followed to prepare supported nanoclusters in UHV conditions.

Metal clusters can be generated in the gas-phase, mass-selected, and then gently deposited on the substrate (either in form of single crystal or thin film). This is a very sophisticated technique, developed in the group of U. Heiz some years ago [129–131,146]. It is based on the production of gas-phase metal clusters in a molecular beam by laser vaporization. The beam contains a fraction of ionized clusters, which can then be separated by mass using a quadrupole mass spectrometer. In this way one obtains a beam of metal clusters all having the same size and the problem becomes that to gently deposit them on the surface (soft landing), in order to prevent damage to the substrate or cluster fragmentation. With this approach one produces truly monodispersed supported metal clusters all having the same size (and possibly also the same shape). Examples of chemical reactivity of supported size-selected metal clusters have been reported, together with an interpretation of the results based on first principle calculations [129,130].

As an alternative, metal clusters can be generated by deposition of the metal from a vapor [146,147]. After impinging on the surface, the metal atoms diffuse and self-aggregate to form clusters of various size, depending on the vaporization rate, substrate temperature, flux, etc. The level of control on the cluster dimensionality is not very high, but it has improved enormously in the last few years and examples of well defined clusters and even of isolated atoms deposited on oxide surfaces using this technique have been reported [146].

Nucleation and growth of metal clusters from self-assembly of deposited atoms is dominated by diffusion of monomers on the surface. Usually diffusion is stopped at point defects where the atoms are more strongly bound and where nucleation and growth occur [148,149]. Theory has been very helpful to gain insight into the mechanisms of deposition and nucleation. Under typical growth conditions, dimers constitute the first step in island nucleation. Atomic-force microscopy (AFM) measurements on the growth of Pd clusters on MgO(100) have shown a constant island density over a wide span of deposition temperatures, typical of defect controlled nucleation [149]. When present, O vacancies at the surface of MgO (F^+ and F centers, see Sect. 4.2), act as strong traps for the metal atoms [129]. However, some authors have suggested that F centers are inefficient for dimerization of late transition metals [150], leaving the question of the sites where Pd nucleates open.

The problem has been addressed in a systematic theoretical study of the dimerization of Pd atoms at various defects on the MgO surface (steps, F and F^+ centers and divacancies [151]). Dimerization is always favorable, although neutral divacancies and F^+ centers exhibit a much stronger tendency to nucleate Pd dimers. This study was based on the simultaneous use of periodic and cluster approaches and constitutes a clear example of the equivalence of the two methods, see Table 1 [151]. It has further demonstrated the role of point defects in the dynamics of nucleation and growth of metal nanoparticles on oxide surfaces.

Table 1 Properties of Pd atoms and dimers adsorbed at regular and defect centers of the MgO surface

		O_{5c}, terrace	O_{4c}, step	F center
$E_a(Pd)^{(a)}$ eV	Cluster	1.50	1.97	4.05
	Periodic	1.36	1.85	3.99
$E_b(Pd-Pd)^{(b)}$ eV	Cluster	0.35	0.54	0.39
	Periodic	0.50	0.66	0.57
R(Pd–Pd), Å	Cluster	2.79	2.63	2.73
	Periodic	2.79	2.63	2.69

(a) $E_a = -E(Pd_1/MgO\_site) + E(Pd) + E(MgO\_site)$
(b) $E_b = -E(Pd_2/MgO\_site) - E(MgO\_O_{5c}) + E(Pd_1/MgO\_site) + E(Pd_1/MgO\_O_{5c})$

6.3 Electronic modifications of metal clusters induced by interaction with a defect

We have seen above (Sect. 4.2) that a variety of defect centers can exist at the surface of an oxide like MgO. Each defect may exhibit a specific effect on the properties of adsorbed species. This becomes particularly important for the chemical reactivity of supported metal atoms and small clusters. In fact, point defects not only act as nucleation centers in the growth of metal clusters (Sect. 6.2), but they can also modify the catalytic activity of the deposited metal particle [129,152,153]. An interesting example is the cyclization reaction of acetylene to form benzene, $3C_2H_2 \rightarrow C_6H_6$, catalyzed by Pd atoms supported on MgO thin film [129,153]. On the MgO(100) surface no benzene is produced. However, even 0.2 monolayers of deposited Pd atoms produce benzene for temperatures of about 215 K. The possibility to catalyze the acetylene trimerization depends critically on the ability of the metal center to coordinate and activate two C_2H_2 molecules and then to bind a C_4H_4 intermediate according to reaction:

$$Pd + 2C_2H_2 \rightarrow Pd(C_2H_2)_2 \rightarrow Pd(C_4H_4) \quad (8)$$

The level of activation of acetylene is clearly larger when a single C_2H_2 is adsorbed, consistent with the idea that the electron density on the metal is essential to promote molecular activation. A key point is therefore the ability of the Pd atom to bind more than one acetylene molecule. Once two acetylene molecules are bound to the

Pd atom, in fact, the formation of the C_4H_4 intermediate occurs with a large energy gain. The following step, $C_4H_4 + C_2H_2 \rightarrow C_6H_6$, requires the capability of the metal center to coordinate and activate a third acetylene molecule according to reaction:

$$Pd(C_4H_4) + C_2H_2 \rightarrow Pd(C_4H_4)(C_2H_2) \rightarrow Pd(C_6H_6) \quad (9)$$

DFT calculations show that the third C_2H_2 molecule interacts very weakly with $Pd(C_4H_4)$ in gas-phase [129,153] and that an isolated Pd atom is not a catalyst for the cyclization process, at variance with the experimental observation for Pd_1/MgO.

Clearly, the MgO support plays a direct role in modifying the properties of the supported Pd atom. A model study where the electronic charge on a Pd atom has been artificially augmented has shown that an excess of charge on Pd reinforces the bonding and the activation of acetylene [129,153]. This shows that the increase of the electron density on Pd is a key mechanism to improve the catalytic properties of the metal atom. Therefore, the role of the substrate must be that to increase the "basic" character of the Pd atoms (or clusters). DFT calculations have shown that the Pd–MgO bond is not characterized by a pronounced charge transfer [154]. However, when Pd is deposited on an O^{2-} ion at a terrace, a step, or a corner site the activation of C_2H_2 is more efficient than for an isolated Pd atom [129]. The donor capability of Pd increases as a function of the adsorption site on MgO in the order terrace<edge<corner, the same trend of surface basicity observed in the CO polimerization reaction [104] (see Sect. 4.2). However, even on the O_{4c}^{2-} and O_{3c}^{2-} anions the Pd atom is not an active catalyst for the cyclotrimerization [129,153]. The increase of electron density on Pd at these sites does not account for the observed reactivity.

Things are different when Pd sits on F and F^+ centers. In this case one can form stable $Pd(C_4H_4)$ complexes, and bind and activate the third acetylene molecule. In addition, the computed energy barriers are broadly consistent with the observed desorption temperature (the barriers are of the order of 1 eV [155], i.e. account for benzene formation between 200 and 300 K).

Much larger barriers are found for other sites. The conclusion is that on F centers a Pd atom becomes an active catalyst for the reaction and that the substrate has a fundamental role in the reactivity of the supported metal. The F centers delocalize in a very effective way the two electrons trapped in the cavity over the adsorbed Pd atom, thus increasing substantially its ability to bind and activate adsorbed hydrocarbon molecules. Thus, F centers not only act as trapping sites of Pd atoms, but they also modify their chemical activity. The same conclusion has been obtained from the study of Au_8 clusters on MgO in the catalytic oxidation of CO to CO_2 [152,156].

6.4 Optical properties of supported metals

The optical response of clusters and nanoparticles is of both fundamental and technological interest in fields like opto-electronics and photochemistry. Due to the discrete electronic structure it is possible in principle to tune the photochemical activity by selectively excite an electronic transition relevant for a given chemical transformation. This can open unexplored possibilities to promote selectively reaction paths by exciting in a specific energy window a cluster of given size and shape.

Cavity Ringdown Spectroscopy (CRDS) allows to study highly diluted systems such as supported clusters due to its high sensitivity. Recently, CRDS has been used to study the visible absorption response of gold atoms and dimers adsorbed on α-SiO_2 [157,158]. The absorption spectrum of $Au_1/\alpha - SiO_2$, Fig. 9, shows two well-resolved transitions at 1.90 and 1.95 eV, a band at 2.48 eV, and another band at 2.75 eV. These bands can be attributed to isolated Au atoms as there is no resemblance with the absorption spectra of Au_n clusters on SiO_2. An intense band at 2.35 eV (inset of Fig. 9) is due to gold dimers, Au_2/SiO_2, and is theoretically predicted at 2.38 eV (see below).

To understand the optical spectrum of Au_1/SiO_2 and Au_2/SiO_2 and to characterize the adsorption sites, cluster model DFT and TD-DFT calculations have been performed. As found for the SiO_2/Mo(112) films (see Sect. 6.1), also on amorphous SiO_2 the Au atoms do not bind to the regular surface sites (Si–O–Si), nor to the isolated, ≡SiOH, or geminal, $=Si(OH)_2$, hydroxyl groups. The fact that cluster growth is not observed experimentally suggests a strong role of surface defects in stabilizing the deposited Au atoms. Several point defects are present in the bulk and on the surface of amorphous silica: Si dangling bonds, $\equiv Si^{\bullet}$ (E' center), non-bridging oxygen, $\equiv Si–O^{\bullet}$ (NBO center), silanolate, $\equiv Si–O^-$ (NBO^- center), O vacancy, ≡Si–Si≡, two-coordinated silicon, =Si:, etc. [159]. Three defect centers, E', NBO, and NBO^-, have been considered in the calculations as possible adsorption sites because of their higher abundance. The binding energies of Au_1 and Au_2 to these defect centers range from 0.9 eV ($\equiv Si–O^-$) to 3.2 eV ($\equiv Si^{\bullet}$), indicating a high sticking probability for Au atoms diffusing on the surface and thermal stability at RT.

From the computed T_e's the two main lines, at 2.48 and 2.75 eV, are attributed to [≡Si–O–Au] (T_e=2.59 eV),

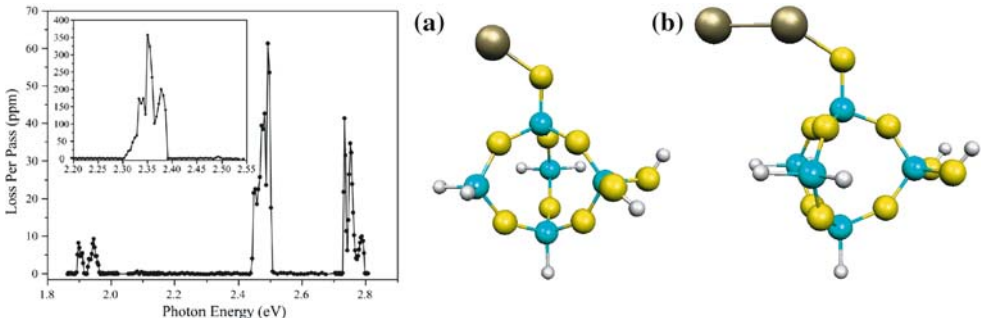

Fig. 9 Absorption spectrum of Au_1 deposited on SiO_2 (*left*). Optimized structures of adsorption complexes on the surface of silica, represented by a $Si_5O_9H_7$ cluster model of edingtonite: **a** Au atom bound to a ≡Si–O• or a ≡Si–O^- defect centre; **b** Au_2 dimer bound to a ≡Si–O• defect centre. Adapted from [157]

and [≡Si–O–Au]$^-$ species (T_e = 2.86 eV). The weak bands around 1.90–1.95 eV are due to low-energy, low-intensity transitions of [≡Si–O–Au] and [≡Si–O–Au]$^-$ (calculated around 2.07–2.26 eV). The peak of moderate intensity at 2.79 eV is due to a weak transition of the neutral [≡Si–O–Au] complex (T_e = 2.99 eV). No other trapping center considered can provide a similar agreement with the measured spectrum.

The conclusion is that Au atoms bind preferentially to ≡Si–O• or ≡Si–O^- defect centers, and that these two types of centers are present in relatively high concentrations on the surface of α-SiO_2. This is further corroborated by the results for Au_2. The computed band for a gold dimer interacting with a NBO centre, ≡Si–O•, 2.38 eV, is very close to that measured for Au_2/SiO_2, 2.35 eV. The transitions for Au_2 bound to a charged ≡Si–O^- defect occur at energies larger than 3.2 eV, and are outside the measured spectral range (1.85–2.82 eV). This study has confirmed the crucial role that point defects have in the stabilization of supported species and has shown the potential of CRDS and TD-DFT to identify the optical properties of supported Au nanoclusters.

7 Summary and conclusions

In the last two decades we have assisted to the rapid development of an area of research known as "scientific computing". This relatively new field complements the more classical experimental approach for the solution of scientific problems. Scientific computing should not be confused with the more general areas of theoretical chemistry or theoretical physics. Experiments produce new facts and discoveries; the role of theory is to provide a general framework for the explanation of the phenomena observed through a series of mathematical laws. Scientific computing is something in between: it is based on well established theories and formalisms but it is used to provide new facts, in a way which becomes more and more similar to the way experiments are performed. Scientific computing has found its way in surface chemistry, material science and nanotechnology.

In this review we have focused our attention on the properties of oxide surfaces, and we have identified the main factors that contribute to determine their behavior: (1) nature of the bonding and electronic structure of the oxide; (2) surface morphology and defectivity; (3) doping and functionalization; (4) redox properties; (5) nanodimensionality (e.g. in ultra-thin films). We have also seen how each of these parameters can affect the properties of supported metal atoms and nanoparticles.

The progress done in this field in the last 10–15 years is impressive. It is largely due to new experimental methods and techniques but the role of theory and computation cannot be underestimated. The possibility to rationalize and even to predict new facts and behaviors thanks to the constant interplay between theory and experiment is an intellectual achievement that can only improve and expand in the future.

Acknowledgements We would like to thank Anna Maria Ferrari, Raffaella Soave, Davide Ricci, Annalisa Del Vitto, Thomas Bredow, Andrea Scagnelli, for their contribution to some of the results presented. The contacts with experimental groups who have regularly exchanged, shared, and discussed their data with us has been an essential source of inspiration: we thank the group of Elio Giamello, Maria Cristina Paganini, and Mario Chiesa at the University of Turin, the group of Ueli Heiz and coworkers at the Technical University of Munich, and that of Hajo Freund, Thomas Risse and Martin Sterrer at the Fritz-Haber Institut in Berlin. We have also profited enormously from exchanges and collaborations with theoreticians: Francesc Illas (University of Barcelona), Notker Rösch (Technical University of Munich), Alex Shluger and Peter Sushko (University College London), Jacek Goniakowski, Alexis Markovitz, and Christian Minot (University of Paris VI), Annabella Selloni (Princeton University), just to mention a few. Finally, we acknowledge the support from the following funding agencies: the Italian MIUR through a Cofin 2005 project, the European Project STRP GSOMEN, the COST Action D41.

References

1. Henry CR (1998) Surf Sci Rep 31:231
2. Renaud G (1998) Surf Sci Rep 32:1
3. Bonnel BA (1998) Prog Surf Sci 57:187
4. Chambers SA (2000) Surf Sci Rep 39:105
5. Bäumer M, Freund HJ (1999) Prog Surf Sci 61:127
6. Lambert RM, Pacchioni G (eds) (1997) Chemisorption and reactivity of supported clusters and thin films. NATO ASI series E, vol. 331. Kluwer, Dordrecht
7. Freund HJ (2002) Surf Sci 500:271
8. Pacchioni G, Bagus PS, Parmigiani F (eds) (1992) Cluster models for surface and bulk phenomena. NATO ASI series B, vol 283, Plenum, New York
9. Kantorovich LN, Holender JM, Gillan MJ (1995) Surf Sci 343:221
10. Castanier E, Noguera C (1996) Surf Sci 364:1
11. Orlando R, Millini R, Perego G, Dovesi R (1997) J Molec Catal A 119:253
12. Leslie M, Gillan MJ (1985) J Phys C 18:973
13. Sauer J, Ugliengo P, Garrone E, Saunders VR (1994) Chem Rev 94:2095
14. Pacchioni G (1995) Heter Chem Rev 2:213
15. Pacchioni G, Frigoli F, Ricci D, Weil JA (2001) Phys Rev B 63:054102
16. The CRYSTAL program is jointly developed by the Theoretical Chemistry Group (Dovesi R, Roetti C, Orlando R, Civalleri B) at the University of Torino and the Computational Materials Science Group (Saunders VR, Harrison NM, Bush IJ), in CLRC, with important contributions from researchers visiting the two laboratories (Zicovich-Wilson CM, Doll K, D'Arco Ph, Llunell M)
17. Ferrari AM, Pacchioni G (1995) J Phys Chem 99:17010
18. Ferrari AM, Pacchioni G (1996) Int J Quant Chem 58:241
19. Nygren MA, Pettersson LGM, Barandiaran Z, Seijo L (1994) J Chem Phys 100:2010
20. Born M (1920) Z Physik 1:45
21. Erbetta D, Ricci D, Pacchioni G (2000) J Chem Phys 113:10744
22. Dick BG, Overhauser AW (1958) Phys Rev 112:90
23. Catlow CRA, Dixon M, Mackrodt WC (1982) In: Catlow CRA (ed) Computer Simulation of Solids, Springer, Berlin p. 130
24. Susko PV, Shluger AL, Catlow CRA (2000) Surf Sci 450: 153
25. Nasluzov VA, Rivanenkov VV, Gordienko AB, Neyman KM, Birkenheuer U, Rösch N (2001) J Chem Phys 115:8157
26. Eichler U, Kölmel CM, Sauer J (1996) Comput Chem 18:463
27. Sierka M, Sauer J (1997) Faraday Discuss 106:41
28. Sherwood P, de Vries A, Collins SJ, Greatbanks SP, Burton NA, Vincent MA, Hiller IH (1997) Faraday Discuss. 106:79
29. Maseras F, Morokuma K (1995) J Comput Chem 16:1170
30. Edwards AH, Sushko PV, Shluger AL et al (2002) IEEE Trans Nucl Sci 49:1383
31. Nasluzov VA, Ivanova EA, Shor AM, Vayssilov GN, Birkenheuer U, Rösch N (2003) J Phys Chem B 107:2228
32. Pacchioni G, Ferrari AM, Bagus PS (1996) Surf Sci 350:159
33. Pople JA, Binkley JS, Seeger R (1976) Int J Quant Chem Symp 10:1
34. Raghavachari K, Pople JA, Replogle ES, Head-Gordon M (1990) J Phys Chem 94:5579
35. Buenker RJ, Peyerimhoff SD, Butscher W (1978) Mol Phys 35:771
36. Pacchioni G, Ieranò G (1998) Phys Rev B 57:818
37. Andersson K, Malmqvist P-Å, Roos BO, Sadlej AJ, Wolinski K (1990) J Phys Chem 94:5483
38. Serrano-Andrés L, Merchán M, Nebot-Gil I, Roos BO, Fülscher M (1993) J Chem Phys 98:3151
39. Di Valentin C, Pacchioni G, Bredow T, Dominguez-Ariza D, Illas F (2002) J Chem Phys 117:2299
40. Illas F, Pacchioni G (1998) J Chem Phys 108:7835
41. Giordano L, Carrasco J, Di Valentin C, Illas F, Pacchioni G (2006) J Chem Phys 124:174709
42. Vosko SH, Wilk L, Nusair M (1980) Can J Phys 58:1200
43. Terakura K, Oguchi T, Williams AR, Klüber J (1984) Phys Rev B 30:4734
44. Shen Z-X, List RS, Dessau DS, Wells BO, Jepsen O, Arko AJ, Barttlet R, Shih CK, Parmigiani F, Huang JC, Lindberg PAP (1991) Phys Rev B 44:3604
45. Perdew JP, Wang Y (1992) Phys Rev B 45:13244
46. Perdew JP, Chevary JA, Vosko SH, Jackson KA, Pederson MR, Singh DJ, Fiolhais C (1992) Phys Rev B 46:6671
47. Perdew JP, Burke K, Ernzerhof M (1996) Phys Rev Lett 77:3865
48. Becke AD (1988) Phys Rev A 38:3098
49. Lee C, Yang W, Parr RG (1988) Phys Rev B 37:785
50. Becke AD (1993) J Chem Phys 98:5648
51. Matxian JM, Irigoras A, Fowler JE, Ugalde JM (2000) Phys Rev A 63:013202
52. Raghavachari K, Ricci D, Pacchioni G (2002) J Chem Phys 116:82
53. Lopez N, Illas F, Rösch N, Pacchioni G (1999) J Chem Phys 110:4873
54. Ranney JT, Starr DE, Musgrove JE, Bald DJ, Campbell CT (1999) Faraday Discuss 114:195
55. Mattsson AE, Jennison DR (2002) Surf Sci 520:L611
56. Hansen KH, Worren T, Stempel S, Laegsgaard E, Baumer M, Freund HJ, Besenbacher F, Stensgaard I (1999) Phys Rev Lett 83:4120
57. Mattsson AE, Kohn W (2001) J Chem Phys 115:3441
58. Nuttall RHD, Weil JA (1981) Can J Phys 59:1696
59. Mombourquette MJ, Weil JA, Mezey PG (1984) Can J Phys 62:21
60. Magagnini M, Giannozzi P, Del Corso A (2000) Phys Rev B 61:2621
61. Laegsgaard J, Stokbro K (2000) Phys Rev B 61:12590
62. Anisimov VI, Zaanen J, Andersen OK (1991) Phys Rev B 44:943
63. Muscat J, Wander A, Harrison NM (2001) Chem Phys Lett 342:397
64. Franchini C, Bayer V, Podloucky R, Paier J, Kresse G (2005) Phys Rev B 72:045132
65. Dohnalek Z, Kimmel GA, McCready DE, Young JS, Dohnalkova A, Smith RS, Kay BD (2002) J Phys Chem B 106:3526
66. Smith DR, Tench AJ (1968) Chem Commun 1113
67. Chiesa M, Paganini MC, Giamello E, Di Valentin C, Pacchioni G (2006) ChemPhysChem 7:728
68. Giamello E, Paganini MC, Murphy DM, Ferrari AM, Pacchioni G (1997) J Phys Chem B 101:971
69. Ricci D, Di Valentin C, Pacchioni G, Sushko PV, Shluger AL, Giamello E (2003) J Am Chem Soc 125:738
70. Chiesa M, Paganini MC, Giamello E, Murphy DM, Di Valentin C, Pacchioni G (2006) Acc Chem Res 39:861
71. Chiesa M, Paganini MC, Giamello E, Di Valentin C, Pacchioni G (2003) Angew Chem Int Ed 42:1759
72. Chiesa M, Paganini MC, Spoto G, Giamello E, Di Valentin C, Del Vitto A, Pacchioni G (2005) J Phys Chem B 109:7314

73. Pacchioni G, Ferrari AM, Giamello E (1996) Chem Phys Lett 255:58
74. Ferrari AM, Pacchioni G (1997) J Chem Phys 107:2066
75. Chiesa M, Martino P, Giamello E, Di Valentin C, Del Vitto A, Pacchioni G (2004) J Phys Chem B 108:11529
76. Ricci D, Pacchioni G, Sushko PV, Shluger A (2003) Surf Sci 542:293
77. Chiesa M, Giamello E, Murphy DM, Pacchioni G, Paganini MC, Soave R, Sojka Z (2001) J Phys Chem B 104:497
78. Blöchl PE (2000) Phys Rev B 62: 6158
79. Weeks RA, Abraham M (1965) J Chem Phys 42:68
80. Kajihara K, Skuja L, Hirano M, Hosono H (2002) Phys Rev Lett 89:135507
81. Di Valentin C, Pacchioni G, Selloni A (2006) Phys Rev Lett 97:166803
82. Stoneham AM (1975) Theory of defects in solids. Oxford University Press, Oxford
83. Tilley RJD (1998) Principles and applications of chemical defects. Stanley Thornes, Cheltenham
84. Pacchioni G (2003) ChemPhysChem 4:1041
85. Wichtendahl R, Rodriguez-Rodrigo R, Härtel U, Kuhlenbeck H, Freund HJ (1999) Surf Sci 423:90
86. Giamello E, Murphy D, Marchese L, Martra G, Zecchina A (1993) J Chem Soc Faraday Trans 89:3715
87. Sterrer M, Heyde M, Novicki M, Nilius N, Risse T, Rust H-P, Pacchioni G, Freund H-J (2006) J Phys Chem B 110:46
88. Pacchioni G, Ieranò G (1997) Phys Rev Lett 79:753
89. Bredow T, Aprà E, Catti M, Pacchioni G (1998) Surf Sci 418:150
90. Bredow T, Pacchioni G (2002) Chem Phys Lett 355:417
91. Spoto G, Gribov N, Ricchiardi G, Damin A, Scarano D, Bordiga S, Lamberti C, Zecchina A (2004) Prog Surf Sci 76:71
92. Pacchioni G (2000) Surf Rev Lett 7:277
93. Zecchina A, Scarano D, Bordiga S, Ricchiardi G, Spoto G, Geobaldo F (1996) Catal Toady 27:403
94. Furuyama S, Fuijii H, Kawamura M, MorimotoT (1978) J Phys Chem 82:1028
95. Spoto G, Gribov E, Damin A, Ricchiardi G, Zecchina A (2003) Surf Sci 540:L605
96. He JW, Estrada CA, Corneille JS, Wu MC, Goodman DW (1992) Surf Sci 261:164
97. Pacchioni G, Minerva T, Bagus PS (1992) Surf Sci 275:450
98. Coluccia S, Marchese M, Marchese L, Martra G, Zecchina A (1993) Spectrochim Acta A 49:1289
99. Pacchioni G, Cogliandro G, Bagus PS (1992) Int J Quant Chem 42:1115
100. Bolis V, Carrato G, Magnaccia G, Morterra C (1998) Thermochim Acta 312:63
101. Zecchina A, Scarano D, Bordiga S, Spoto G, Lamberti C (2001) Adv Catal 46:265
102. Che M, Tench AJ (1982) Adv Catal 31:78
103. Pacchioni G, Ricart JM, Illas F (1994) J Am Chem Soc 116:10152
104. Di Valentin C, Finazzi E, Pacchioni G (2005) Surf Sci 591:70
105. Kapteijn F, Rodriguez-Mirasol J, Moulijn JA (1996) Appl Catal B Environ 9:25
106. Drago RS, Jurczyk K, Kob N (1997) Appl Catal B Environ 13:69
107. Izumi Y, Shimizu T, Kobayashi T, Aika K (2000) Chem Commun 12:1053
108. Scagnelli A, Di Valentin C, Pacchioni G (2006) Surf Sci 600:386
109. Zemva P, Lesar A, Senegacnik M, Kobal I (2000) Phys Chem Chem Phys 2:3319
110. Vijay A, Mills G, Metiu HJ (2003) Chem Phys 118:6536
111. Wahlstrom E, Lopez N, Schaub R, Thostrup P, Ronnau A, Africh C, Laegsgaard E, Norskov JK, Besenbacher F (2003) Phys Rev Lett 90:026101
112. Meier DC, Goodman DW (2004) J Am Chem Soc 126:1892
113. Lee SS, Fan CY, Wu TP, Anderson SL (2004) J Am Chem Soc 126:5682
114. Boccuzzi F, Chiorino A, Manzoli M (2002) Surf Sci 502–503:513
115. Vittadini A, Selloni A (2002) J Chem Phys 117:353
116. Haruta M (1997) Catal Today 36:153
117. Wörz AS, Heiz U, Cinquini F, Pacchioni G (2005) J Phys Chem B 109:18418
118. Neumaier M, Weigend F, Hampe O, Kappes MM (2005) J Chem Phys 122:104702
119. Schintke S, Schneider W-D (2004) J Phys Condens Matter 16:R49
120. Pacchioni G, Giordano L, Baistrocchi M (2005) Phys Rev Lett 94:226104
121. Repp J, Meyer G, Olsson FE, Persson M (2004) Science 305:493
122. Giordano L, Pacchioni G (2006) Phys Chem Chem Phys 8:3335
123. Kulawik M, Nilius N, Freund HJ (2006) Phys Rev Lett 96:036103
124. Giordano L, Cinquini F, Pacchioni G (2006) Phys Rev B 73:045414
125. Krischok S, Stracke P, Höfft O, Kempter V, Zhukovskii YF, Kotomin EA (2006) Surf Sci 600:3815
126. Wendt S, Ozensoy E, Wei T, Frerichs M, Cai Y, Chen MS, Goodman DW (2005) Phys Rev B 72:115409
127. Schmid G, Bäumle M, Geerkens M, Heim I, Osemann C, Sawitowski T (1999) Chem Soc Rev 28:179
128. Campbell CT (1997) Surf Sci Rep 27:1
129. Abbet S, Sanchez A, Heiz U, Schneider WD, Ferrari AM, Pacchioni G, Rösch N (2000) J Am Chem Soc 122:3453
130. Judai K, Wörz A, Abbet S, Heiz U, Del Vitto A, Giordano L, Pacchioni G (2005) Phys Chem Chem Phys 7:955
131. Abbet S, Heiz U, Häkkinen H, Landman U (2001) Phys Rev Lett 86:5950
132. Frank M, Bäumer M (2000) Phys Chem Chem Phys 2:3723
133. Sterrer M, Risse T, Freund H-J, Carrasco J, Illas F, Di Valentin C, Giordano L, Pacchioni G (2006) Angew Chemie Int Ed 45:2633
134. Chiesa M, Giamello E, Paganini MC, Pacchioni G, Soave R, Murphy DM, Sojka ZJ (2001) J Phys Chem B 105:497
135. Chiesa M, Giamello E, Di Valentin C, Pacchioni G, Sojka Z, Van Doorsiaer S (2005) J Am Chem Soc 127:16935
136. Yulikov M, Sterrer M, Heyde M, Rust H-P, Risse T, Freund HJ, Pacchioni G, Scagnelli A (2006) Phys Rev Lett 96:146804
137. te Velde G, Bickelhaupt FM, Baerends EJ, Fonseca Guerra C, van Gisbergen SJA, Snijders JG, Ziegler T (2001) J Comp Chem 22:931
138. Giordano L, Del Vitto A, Pacchioni G (2006) J Chem Phys 124:034701
139. Xe X, Goodman DW (1993) Surf Sci 282:323
140. Schroeder T, Giorgi JB, Bäumer M, Freund HJ (2002) Phys Rev B 66:165422
141. Giordano L, Ricci D, Pacchioni G, Ugliengo P (2005) Surf Sci 584:225
142. Weissenrieder J, Kaya S, Lu JL, Gao HJ, Shaikhutdinov S, Freund H–J, Sierka M, Todorova TK, Sauer J (2005) Phys Rev Lett 95:076103
143. Wallace WT, Min BK, Goodman DW (2005) J Mol Catal A 228:3

144. Min BK, Wallace WT, Goodman DW (2004) J Phys Chem B 108:14609
145. Ozensoy E, Min BK, Santra AK, Goodman DW (2004) J Phys Chem B 108:4351
146. Binnis C (2001) Surf Sci Reports 44:1
147. Franck M, Bäumer M (2000) Phys Chem Chem Phys 2:3723
148. Frank M, Baumer M, Kuhnemuth R, Freund HJ (2001) J Phys Chem B 105:8569
149. Haas G, Menck A, Brune H, Barth JV, Venables JA, Kern K (2000) Phys Rev B 61:11105
150. Bogicevic A, Jennison DR (1999) Surf Sci 437:L741; ibidem (2002) 515:L481
151. Giordano L, Di Valentin C, Goniakowski J, Pacchioni G (2004) Phys Rev Lett 92:096105
152. Sanchez A, Abbet S, Heiz U, Schneider WD, Häkkinen H, Barnett RN, Landman U (1999) J Phys Chem A 103:9573
153. Sanchez A, Abbet S, Heiz U, Schneider WD, Ferrari AM, Pacchioni G, Rösch N (2000) Surf Sci 454/456:984
154. Yudanov I, Pacchioni G, Neyman K, Rösch N (1997) J Phys Chem 101:2786
155. Ferrari AM, Giordano L, Rösch N, Heiz U, Abbet S, Sanchez A, Pacchioni G (2000) J Phys Chem B 104:10612
156. Yoon B, Häkkinen H, Landman U, Wörz AS, Antonietti JM, Abbet S, Judai K, Heiz U, (2005) Science 307:403
157. Antonietti J-M, Michalski M, Heiz U, Jones H, Lim KH, Rösch N, Del Vitto A, Pacchioni G (2005) Phys Rev Lett 94:213402
158. Del Vitto A, Pacchioni G, Lim KH, Rösch N, Antonietti J-M, Michalski M, Heiz U, Jones H (2005) J Phys Chem B 109:19876
159. Pacchioni G, Skuja L, Griscom DL (eds) (2000) Defects in SiO_2 and related dielectrics: science and technology. NATO science series. Kluwer, Dordrecht